

Unsupervised Scale-Invariant Multispectral Shape Matching

Idan Pazi
Tel Aviv University

idan.pazi@outlook.com

Dvir Ginzburg
Tel Aviv University

dvirginzburg@mail.tau.ac.il

Dan Raviv
Tel Aviv University

darav@tauex.tau.ac.il

Abstract

Alignment between non-rigid stretchable structures is one of the hardest tasks in computer vision, as the invariant properties are hard to define on one hand, and on the other hand no labelled data exists for real datasets. We present unsupervised neural network architecture based upon the spectrum of scale-invariant geometry. We build atop the functional maps architecture, but show that learning local features, as done until now, is not enough once the isometric assumption breaks but can be solved using scale-invariant geometry. Our method is agnostic to local-scale deformations and shows superior performance for matching shapes from different domains when compared to existing spectral state-of-the-art solutions.

1. Introduction

Shape correspondence is the problem of aligning two shapes and finding a point-to-point map between them. Non-rigid shape correspondence, where stretching and bending allowed, can be viewed as revealing the common anatomy between arbitrary shapes. This alignment problem is fundamental yet challenging in 3D space [9]. The solution to this problem and its derivatives is vital for many applications, such as texture transfer, pose transfer, and 3D scanning [42, 41]. Research in the field of shape correspondence has found the general non-rigid problem to be incredibly tricky, as the invariant properties are non-trivial to define. Trying to solve this problem directly, matching point by point on the spatial domain gives a vast solution space, non-convex, and highly non-linear [25, 21]. The complexity of non-rigid shape correspondence problems led the efforts in this field to simplify the problem, primarily by exploiting invariants between shapes [5], focusing on metric-based methods such as isometry and near-isometry assumptions [10, 24]. The success of metric based approach, with comparison to previous efforts, is based on the fundamental understanding that the features and the algorithms need to operate on the manifold itself and not on the ambient space. Finding appropriate descriptors for detecting

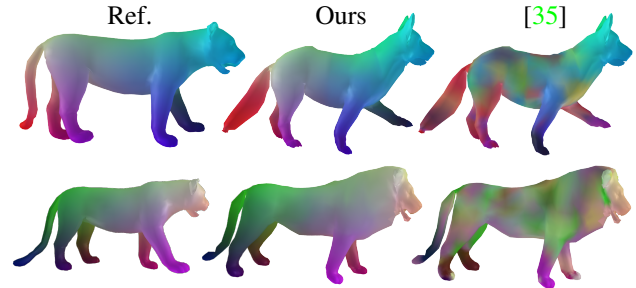


Figure 1. Unsupervised functional maps correspondence between highly non-isometric shapes from the SMAL dataset

signatures that are invariant to non-rigid deformations is not an easy task. Kernel methods such as the Heat Kernel Signature [40] and the Wave Kernel Signature [3] were highly useful; these descriptors rely on the intrinsic geometry of the shapes and are inherently invariant to isometries. Prominent *Local Reference* methods analyze descriptors from the point of view of small patches on the shape and thus invariant to rotations [19]. On each reference patch, a descriptive and unique signature can be extracted using hand-crafted algorithms such as accumulating vertices normals [38] or curvatures [44]. Recent works show a significant improvement of descriptors by applying machine learning tools for filtering given descriptors [22] and using extracted features as descriptors [12].

Spectral domain methods for shape correspondence had increased popularity in recent years, commonly using the Laplace-Beltrami operator (LBO) eigendecomposition for spanning the spectral domain. The eigenfunctions of the LBO exhibit a set of appealing properties; it has an orthonormal complete set, and it is the optimal basis for projecting functions on shapes [1]. Functional maps framework laid the foundations of recent advancement in spectral-domain methods. In [27], Ovsjanikov *et al.* showed it is possible to find a linear transformation between the spectrums of different shapes. Such linear transformation leads to efficient optimization of the descriptors correspondence problem, shifting the problem from estimating similarity between descriptors on the complex spatial domain

to solving a least-squares problem in a compact spectral domain. Later works show how functional maps could be utilized in deep-learning architectures and outperform other methods on standard shape correspondence benchmarks [22, 16, 35, 12].

Alas, the theoretical foundations for the existence of a linear map between LBO decompositions assume isometry between shapes. Perfect isometry between non-deformable shapes does not hold for the general non-rigid shape correspondence problem. Still, experiments show that on the near-isometric case, such as pose changes and the correspondence of subjects from the same domain (e.g., humans), the Laplace-Beltrami operator leads to a good generalization and manage to provide excellent correspondence when compared to other non-spectral methods.

So far, most of the functional maps research focus on matching near-isometric shapes with similar local and global properties, and only several attempts were made to correspond non-isometric shapes using spectral-domain methods. The cyclic distortion was introduced in [15], neglecting the need for a consistent metric between shapes and successfully correspond stretchable domains. A Genetic algorithm was introduced in [13], where the correct correspondence iteratively evolves based on landmark descriptors and the functional maps framework. On the research for non-isometric descriptors, scale-invariant kernel purposed in [11], formulating descriptors that are invariant to global and local scale.

Aflalo *et al.* presented in [2] a scale-invariant metric that is mathematically consistent under global scaling and contributes to the invariancy of the LBO under local scaling. One can argue that non-isometric shapes differ by a set of affine transformations and can be approximated by such finite set; by inducing a scale-invariant metric we can treat the shapes as near-isometric, assuming a distance preserving map exists between the shapes when measured by the alternative pseudo-metric.

In functional based methods described above, the basis functions were derived using a Euclidean Laplace Beltrami Operator which vary significantly during non-isometric deformations and tried to cope with that by learning local features per point. We propose to relax the isometric constraints of functional maps by introducing a multispectral strategy based on scale-invariant assumptions. We show how such an approach improves the performance on standard benchmarks and open new possibilities to match non-isometric shapes using functional maps.

2. Contributions

- We introduce a new functional maps architecture for non-rigid model alignment based on multispectral scale-invariant strategy.

- We report improved alignment results on multiple non-rigid benchmarks based on isometric or near-isometric invariants.
- Provide superior alignment results, by a large margin, on scenarios where extensive stretching exists.

3. Background

3.1. Riemann Manifold

We consider a Riemann manifold (\mathcal{X}, g) in the 3-dimensional space as a parametrized surface $\mathcal{X} : \Omega_{\mathcal{X}} \subset \mathbb{R}^2 \rightarrow \mathbb{R}^3$ with the metric g varies differentiably with $p \in \Omega_{\mathcal{X}}$. The metric g can be viewed as a family of inner products $g_p(p_1, p_2) = \langle p_1, p_2 \rangle_p$ between vectors p_1, p_2 in the neighborhood of p . A map T from one Riemann manifolds \mathcal{X} to another manifold \mathcal{Y} is a function that maps every point from one shape to the other $T : \Omega_{\mathcal{X}} \rightarrow \Omega_{\mathcal{Y}}$. Two Riemann manifolds are *isometric* if there is a map between them that preserves the distance between points measured by their induced metrics.

3.2. Laplace-Beltrami operator spectral domain

Let $f : \Omega_{\mathcal{X}} \rightarrow \mathbb{R}$, a differentiable function over a manifold that associates a scalar to every point on the manifold. The *Laplace-Beltrami operator* on f defined as:

$$\Delta_g f = -\frac{1}{\sqrt{\det g}} \sum_{ij} \frac{\partial}{\partial x_i} (g^{-1} \sqrt{\det g} \frac{\partial}{\partial x_j} f) \quad (1)$$

with x_1, x_2 coordinates in $\Omega_{\mathcal{X}}$ and g is the metric tensor $g = \begin{pmatrix} g_{11} & g_{12} \\ g_{12} & g_{22} \end{pmatrix}$, $g_{ij} = \langle p_i, p_j \rangle_p$. Hence, the operator is fully defined by the metric tensor g . It is a positive semi-definite operator and admits an eigendecomposition of an orthonormal basis:

$$\begin{aligned} \Delta_g \phi_i &= \lambda_i \phi_i \\ \langle \phi_i, \phi_j \rangle &= \delta_{ij} \end{aligned} \quad (2)$$

Equipped with this orthonormal basis of eigenfunctions, we can represent any function on the manifold as a Fourier series:

$$f = \sum \langle \phi_i, f \rangle_{\mathcal{X}} \phi_i \quad (3)$$

It has been shown in [1] that the first k eigenfunctions of the LBO decomposition are the optimal k -dimensional basis for representing functions on \mathcal{X} .

3.3. Scale-invariant geometry

Aflalo *et al.* in [2] built a metric on a parameterized differentiable surface that would be invariant for scaling. They showed that such metric \tilde{g} could be achieved if we adjust the Euclidean metric g by the magnitude of the Gaussian curvature K :

$$\tilde{g} = |K| g \quad (4)$$

It can be shown that \tilde{g} is scale and isometric invariant, meaning that distances on the surface \mathcal{X} preserved when locally scaled by some factor. An intuitive example is a simple arc length along a sphere where the Gaussian curvature is the reciprocal of the radius, inversely changes upon scaling. This pseudo-metric can be used to define a scale-invariant Laplace Beltrami operator $\Delta_{\tilde{g}}$ by substituting into eq (1).

3.4. Functional maps

Functional maps [27, 28], are representations of maps between pairs of shapes that allows efficient inference and manipulation. Given two manifolds $\mathcal{X} : \Omega_{\mathcal{X}} \subset \mathbb{R}^2 \rightarrow \mathbb{R}^3$ and $\mathcal{Y} : \Omega_{\mathcal{Y}} \subset \mathbb{R}^2 \rightarrow \mathbb{R}^3$, with the spaces of real valued functions on the domains, $\mathcal{F}(\Omega_{\mathcal{X}}, \mathbb{R})$ and $\mathcal{F}(\Omega_{\mathcal{Y}}, \mathbb{R})$, our goal is to represent a bijective mapping between the two manifolds, namely $T : \Omega_{\mathcal{X}} \rightarrow \Omega_{\mathcal{Y}}$. Given some scalar function $f : \Omega_{\mathcal{X}} \rightarrow \mathbb{R}$ on the first manifold, we may apply the mapping to obtain a corresponding function on the second manifold by $f \circ T^{-1} : \Omega_{\mathcal{Y}} \rightarrow \mathbb{R}$, this function composition can be viewed as a function transformation, represented by $T_F : \mathcal{F}(\Omega_{\mathcal{X}}, \mathbb{R}) \rightarrow \mathcal{F}(\Omega_{\mathcal{Y}}, \mathbb{R})$. The goal mapping T can be recovered from the function transformation T_F by applying T_F on a set of indicator functions with a single point support for every point in the domain. As opposed to the complex non-linear mapping T , the functional transformation T_F is a linear map between function spaces. Now we assume the function spaces $\mathcal{F}(\Omega_{\mathcal{X}}, \mathbb{R})$ and $\mathcal{F}(\Omega_{\mathcal{Y}}, \mathbb{R})$ have orthonormal basis Φ and Ψ respectively, so any function $f : \Omega_{\mathcal{X}} \rightarrow \mathbb{R}$ can be represented as a linear combination $f = \sum_i a_i \phi_i$, then we can show the following:

$$T_F(f) = T_F \left(\sum_i a_i \phi_i \right) = \sum_i a_i T_F(\phi_i) = \sum_i \sum_j a_i c_{ij} \psi_j \quad (5)$$

Where c_{ij} is the j 'th coefficient in the basis span by Ψ of the transformation of the i 'th basis function, hence $T_F(\phi_i) = \sum_j c_{ij} \psi_j$, meaning that $T_F(\phi_i)$ determined only by the basis and the map T . When choosing orthonormal basis functions we may use the inner product for getting $c_{ij} = \langle T_F(\phi_i), \psi_j \rangle$. If we represent c_{ij} elements in matrix C and f as a vector of the coefficients $\vec{a} = (a_0, a_1, \dots, a_i, \dots)$, then we can reformulate eq (5):

$$T_F(\vec{a}) = C\vec{a} \quad (6)$$

Under the following framework of functional maps, the problem of shape matching using descriptors of two shapes can be transformed from non-convex highly non-linear constraints about every point in each of the shapes to a linear least squares problem over the elements of the matrix C . Given a set of descriptors on each shape F and G and their projection to the spectral domains - F_{Φ} and G_{Ψ} , finding

$C_{\Phi\Psi}$, a linear transformation from the spectral domain Φ to Ψ , is a least-squares problem:

$$C_{\Phi\Psi} = \underset{C}{\operatorname{argmin}} \|CF_{\Phi} - G_{\Psi}\|_F^2 \quad (7)$$

An inverse transformation $C_{\Psi\Phi}$ can be achieved by replacing F_{Φ} and G_{Ψ} . It has been shown that C of size significantly small compared to the number of vertices can successfully describe the full correspondence with low error when the LBO is used to span the spectral domain on each shape [27, 32, 18, 29].

So far, the research in the field of functional maps used the standard Laplace-Beltrami Operator decomposition (LBO) with the Euclidean metric as the basis of choice. The choice of basis is a fundamental component for the solution, as each shape descriptor is projected into it, and the capacity of C to efficiently describe complex structures is derived from the strength of the space spanned by the basis. Choosing the LBO basis imposes an assumption of isometry between the matched shapes, which is required for comparing the two bases. In this work, the limitations of this choice are researched and relaxed by using an alternative scale-invariant LBO.

3.5. Deep functional maps

By using the functional maps framework, Litany *et al.* made a paradigm shift in FMNet [22], by training a neural network for solving the shape correspondence problem without solving a labeling problem for each point but by a refinement of baseline SHOT descriptors per point. In this architecture, the descriptors are optimized for solving the correspondence in the spectral domain, trained to describe the given dataset successfully. For training the network, a soft error loss term is introduced, estimates the geodesic distance loss at each point for a given functional map C using the ground truth correspondence and the geodesic distances between points on each shape.

3.6. Unsupervised deep functional maps

In SURFMNet [35], a more axiomatic approach is suggested, where a set of numerical properties of the C matrix have been shown to have a strong correlation to the desired ground-truth in terms of the geodesic distance. A composite of loss terms on the map C , forcing orthogonality and commutatively, showed superb alignment results [26]. Not only this architecture is fully unsupervised and reduce the need for expensive point labeling, but it is also completely independent on the geodesic distances on the shapes, which make this architecture compelling for corresponding non-isometry shapes where the geodesic distance between corresponding points on the shapes may differ significantly. A different approach suggested by Ginzburg and Raviv [15], focused on a cyclic architecture, where the distortion was

measured only in the source domain. Not only were they able to show some resistance to stretching, but that was a fully unsupervised pipeline.

4. Method

In this work, we facilitate a scale-invariant geometry for non-isometric shape correspondence. We are basing our method on recent deep learning spectral-domain architectures. First, we describe how we construct the deep local descriptors, following a walkthrough for building the scale-invariant multi-spectrum. We further explain how we integrated the different basis functions in one pipeline to infer a pointwise correlation matrix. The full architecture of our solution is presented in Figure 3.

4.1. Descriptors

We have used the FMNet [22] deep learning paradigm for generating local descriptors on the shapes. On the pre-processing stage, we create the baseline descriptors using the hand-crafted SHOT algorithm [38] where 352 initial descriptors are generated per point for each shape. During training and inference, each set of descriptors is filtered through a series of 7 fully connected residual layers[17], with shared weights between the two shapes. We wish to emphasize that we left the descriptors path unchanged - our architecture bear the same amount of learned weights as in the other architectures we compare it against [16, 35]. However, our generated descriptors are more informative, thanks to evaluating their performance on richer spectral domains when training.

4.2. Scale-invariant spectral domain

Experiments shows that while the regular LBO decomposition encapsulates the global structure of the shape, inducing scale-invariant geometry impair the global properties of the decomposition. To overcome this problem, Aflalo *et al.* [1] introduced $\alpha \in [0, 1]$ exponent parameter on the curvature to interpolate between the Euclidean metric ($\alpha = 0$) to the scale-invariant pseudo-metric ($\alpha = 1$), defining an intermediate scale-invariant geometry:

$$\tilde{g}_\alpha = |K|^\alpha \langle S_{\omega_i}, S_{\omega_j} \rangle \quad (8)$$

A visualization of the impact of α on the spectral domain is shown in Figure 2. In [8] the choice of α was proven to be an essential ingredient for the success of the correspondence and was optimized for each pair of shapes. Estimating the Gaussian curvature on a triangular mesh is still under active research [23], due to limitations of the discrete representation [7]. Here, we estimated the Gaussian curvature of the manifolds by first smoothing the surface using the method described in [43], then the Gaussian curvature

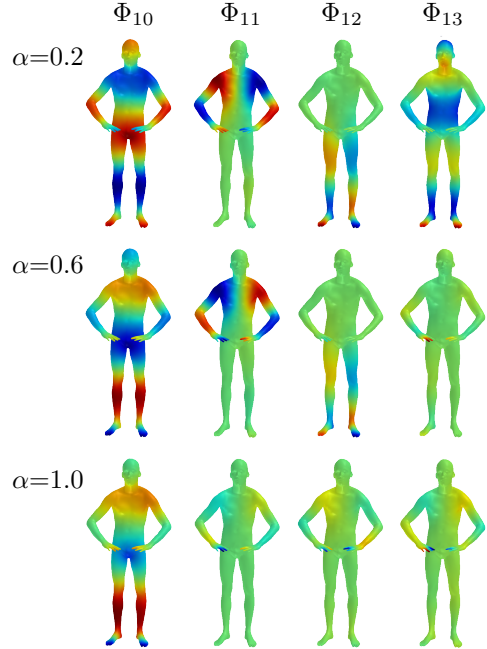


Figure 2. The 10th to 13th eigenfunctions of the intermediate scale-invariant LBO with different α values. As we tend to more scale-invariant metric (higher α), the spectrum concentrate on local features, even on relatively low frequencies.

was estimated using the method described in [36], and further processed by clipping the curvature for setting a minimal curvature, avoiding vanishing distances on flat areas[2] and trimmed the curvature for setting maximal curvature to reduce the quantization noise of small triangles.

4.3. Discrete scale-invariant LBO

The general approach for the discretization of the LBO on a triangulated surface with vertices $\{\vec{v}_i\}_{i=0}^{n-1}$ each with immediate neighbors $\{N(i)\}_{i=0}^{n-1}$ is to represent the operator as:

$$\Delta f(\vec{v}_i) := \frac{1}{d_i} \sum_{j \in N(i)} w_{ij} (f(\vec{v}_i) - f(\vec{v}_j)) \quad (9)$$

With some *mass* d_i associated to each vertex and a *weight* w_{ij} associated to each edge. Popular weights implementation is the cotangent weights:

$$w_{ij} = \frac{\cot(\alpha_{ij}) + \cot(\beta_{ij})}{2} \quad (10)$$

where α_{ij} and β_{ij} denote the two angles opposite to the edge (i, j). We use the cotangent weights and mass $d_i = a(i)/3$ where $a(i)$ is the scale-invariant area of all triangles at vertex i . We have based our implementation on the finite-element approach by Reuter *et al.* [31] The implementation achieves numerical stability by formulating the problem as a generalized eigenvalues problem:

$$A\vec{\phi} = -\lambda B\vec{\phi} \quad (11)$$

Where A is the stiffness matrix of the graph:

$$A(i, j) := \begin{cases} \frac{\cot(\alpha_{ij}) + \cot(\beta_{ij})}{2} & (i, j) \text{ edge} \\ -\sum_{k \in N(i)} A(i, k) & i = j \\ 0 & \text{otherwise} \end{cases} \quad (12)$$

and B is the mass matrix:

$$B(i, j) := \begin{cases} \frac{|K_1|^\alpha |t_1| + |K_2|^\alpha |t_2|}{12} & (i, j) \text{ edge} \\ \frac{\sum_{l \in N(i)} |K_l|^\alpha |t_l|}{6} & i = j \\ 0 & \text{otherwise} \end{cases} \quad (13)$$

$|t_i|$ is the area of the triangle t_i , K_i is the Gaussian curvature associated to the triangle t_i where t_1, t_2 are the triangles that share the edge (i, j) , α is the interpolation parameter from eq (8).

4.4. Loss function

Our loss function follows the unsupervised loss term presented in SURFMNet[35], where a set of regularization terms applied on the functional maps $C_{\Phi\Psi}$ and $C_{\Psi\Phi}$ from the optimization problem defined in eq (7).

Bijectivity of the transformation can be achieved by enforcing identity for the transformation from one spectral domain to the other and back:

$$E_1 = \|C_{\Phi\Psi}C_{\Psi\Phi} - I\|_2^2 + \|C_{\Psi\Phi}C_{\Phi\Psi} - I\|_2^2 \quad (14)$$

Area preservation can be enforced by the orthogonality of each transformation:

$$E_2 = \|C_{\Phi\Psi}^\top C_{\Phi\Psi} - I\|_2^2 + \|C_{\Psi\Phi}^\top C_{\Psi\Phi} - I\|_2^2 \quad (15)$$

Pointwise map express an intrinsic isometry if and only if the associated functional map commutes with the Laplace Beltrami operator [27, 34]. This can be enforced by commutativity of the functional map with the Laplacian:

$$E_3 = \|C_{\Phi\Psi}\Lambda_\Phi - \Lambda_\Psi C_{\Phi\Psi}\|^2 + \|C_{\Psi\Phi}\Lambda_\Psi - \Lambda_\Phi C_{\Psi\Phi}\|^2 \quad (16)$$

where Λ_Φ and Λ_Ψ are diagonal matrices of the eigenvalues of Φ and Ψ respectfully.

Functional map T can represent a pointwise map if and only if it preserves the pointwise product \odot between functions, namely $T(f \odot g) = T(f) \odot T(g)$ [39]. Nogneng and Ovsjanikov followed this observation in [26] to present a penalty for descriptor preservation via commutativity:

$$E_4 = \sum_{f_i \in F_\Phi; g_i \in G_\Phi} \|C_{\Phi\Psi}M_{f_i} - M_{g_i}C_{\Phi\Psi}\|^2 + \|C_{\Psi\Phi}M_{g_i} - M_{f_i}C_{\Psi\Phi}\|^2, \quad (17)$$

$$M_{f_i} = \Phi^+ \text{Diag}(f_i) \Phi$$

$$M_{g_i} = \Psi^+ \text{Diag}(g_i) \Psi$$

Where F_Φ and G_Ψ are the descriptors of the shapes with the spectral domains Φ and Ψ respectfully, and $+$ is the Moore-Penrose pseudoinverse.

Our architecture outputs a set of functional maps $Sp = \{(C_{\Phi_s\Psi_s}, C_{\Psi_s\Phi_s})\}_{s=1}^k$ for each of the k spectral domain pairs $\Phi_s\Psi_s$. our loss functions accumulate loss over all spectrums:

$$E = \sum_{C_{\Phi_s\Psi_s}, C_{\Psi_s\Phi_s} \in Sp} \sum_{i \in \{1,2,3,4\}} w_i E_i(C_{\Phi_s\Psi_s}, C_{\Psi_s\Phi_s}) \quad (18)$$

The loss function is differentiable with respect to the functional maps and allows unsupervised network training without a need for the ground-truth correspondence, measuring expensive geodesic distances on shapes or even inferring the pointwise correspondence from maps. It has been shown in [35] that this loss term is correlated to the desired low geodesic error of the pointwise correspondence. Unlike other works that presented similar penalties on the functional maps [27, 37, 14], the structural penalty on the functional maps is decoupled from the descriptor similarity optimization of eq (7).

4.5. Pointwise correspondence from multispectral functional map

Even after obtaining the functional map C between two spectral domains, the task of finding the pointwise correspondence between shapes is still not trivial [33].

In [27], an efficient method to find the pointwise correspondence is presented, based upon proximity search in the spectral domain. Given spectral domains for each shape represented by matrices Φ and Ψ , where each column corresponds to a point and each row to an eigenfunction. For vertex i on Ψ , the corresponding point on Φ is the nearest neighbor in the spectral domain:

$$Corr(i) = \underset{j}{\operatorname{argmin}} \|col_j(C\Phi) - col_i(\Psi)\|_2 \quad (19)$$

Where $Corr(i)$ is the index of the corresponding vertex to the i 'th vertex and $col_i(M)$ is the i 'th column of the matrix M . Using multispectral maps we wish to blend the correspondence information and infer a single match using multiple pairs of spectral domains Φ_s and Ψ_s with functional map C_s between them. Direct proximity search within all spectral domains is not possible since distances between domains are not directly comparable. We have found that the optimal correspondence can be established by normalizing the mean and range of all distances in the different spectral domains and selecting the correspondence giving the optimal normalized distance:

$$Corr(i) = \underset{j}{\operatorname{argmin}} \min_s \|col_j(C_s\Phi_s) - col_i(\Psi_s)\|_2^* \quad (20)$$

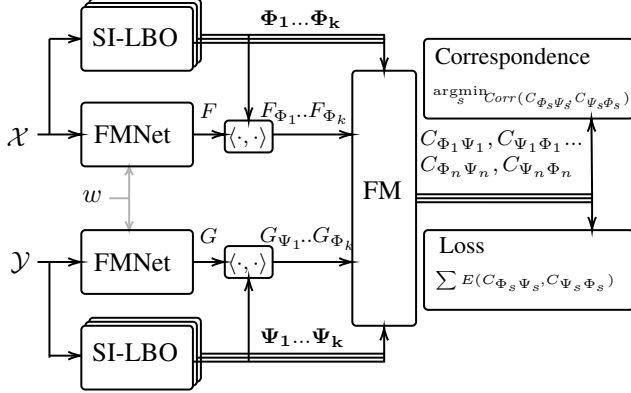


Figure 3. Multispectral deep functional maps architecture. Given two manifolds \mathcal{X} and \mathcal{Y} , for each shape we span a set of spectral domains $\{\Phi_s\}$ $\{\Psi_s\}$ and we infer descriptors F , G using FMNet architecture. Functional maps correspondence between the descriptors is done on each spectral domain yielding a set of linear transformations between the spectral domains of each shape (on both directions) $\{C_{\Phi_s \Psi_s}\}$ $\{C_{\Psi_s \Phi_s}\}$. The loss accumulated over all transformations, the correspondence deduced according to eq (20). Pointwise correspondence from the functional map is extracted on inference.

Where $\|\cdot\|_2^*$ is the L_2 distance with the following normalization, on each spectrum we do a linear normalization of the distances to $[0, 1]$ and then subtracting the mean of all the distances in the spectral domain, establishing a comparable distance between spectrums. By fusing the correspondences we can compensate for the degraded local performance of scale-invariant metrics while withstanding non-isometric deformations.

4.6. Parameters

On the preprocessing stage, we have created three different spectral domains for each shape, defined by choosing the intermediate metric factor α heuristically, for the near-isometric datasets we have used $[0, 0.6, 0.8]$ and for the non-isometric datasets we have used $[0.5, 0.6, 0.8]$. The Gaussian curvature clipping was made to the 0.4% - 75% range on each shape.

5. Experiments

We have tested our method on different datasets that show how we improve over recent state-of-the-art solutions and highlight the strength of our framework.

5.1. Error evaluation

For evaluating the performance of our method and comparing against other methods, we have used the Princeton benchmark [20]. Given the ground truth map between two shapes $T : \Omega_{\mathcal{X}} \rightarrow \Omega_{\mathcal{Y}}$, and estimation of that mapping \hat{T} the geodesic error for each point is the geodesic distance

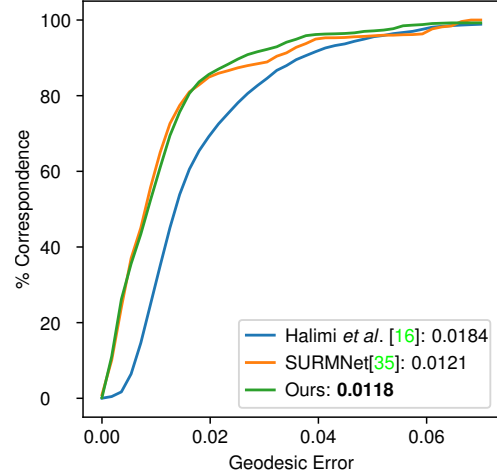


Figure 4. Error evaluation on FAUST dataset comparing our implementations to SURFMNet [35] on inter-subject and intra-subjects cases. Our multispectral architecture shows improvement even on the near-isometric benchmark

between the two mappings, and the total measure of error is the sum of all geodesic errors divided by the area of the target figure:

$$\epsilon(\hat{T}) = \sum_{x \in \mathcal{X}} \frac{\mathcal{D}_{\mathcal{Y}}(T(x), \hat{T}(x))}{\sqrt{\text{area}(\mathcal{Y})}}, \quad (21)$$

Where $\mathcal{D}_{\mathcal{Y}}$ is the geodesic distance between two points on \mathcal{Y} .

5.2. Synthetic FAUST

For evaluating our method on the near-isometry case, we compared our method to [35] and [16] on the synthetic FAUST dataset [6]. It contains synthetic scans of 10 different human subjects, each on 10 different poses (100 shapes in total). As suggested in [22], we trained our model on the 80 shapes from the first 8 subjects and tested on the rest 20 shapes. In Figure 4 we present the geodesic error comparison. Even on the near-isometry case, which our method was not optimized for, we manage to outperform state-of-the-art solutions optimized specifically for this case. We show that the isometry assumption on recent spectral domain methods is not only limiting the capabilities of such methods to correspond shapes from different domains, but also has an impact on the near-isometry case, where these methods are sensitive to the stretching between different poses and different subjects.

5.3. Locally scaled FAUST

To highlight the ability of our method to tolerate deformations and the sensitivity of current methods to non-

isometry cases, we have conducted the following experiment. We locally scaled examples from the FAUST dataset, and applied the scaling to the SHOT descriptors as well, simulating a perfect scale-invariant descriptors. We have deformed the shapes by applying local uniform scaling of different parts of the bodies, such as head, arms, legs, and hands while keeping the shapes smooth as possible. The dataset preserved many of the characteristics of the original FAUST dataset and was designed to only stress the ability of spectral methods to handle local scaling while keeping most of the parameters optimized to the nature of the dataset.

We compared the performance of SURFMNet[35] using the standard LBO and using a single scale invariant spectrum ($\alpha=0.6$) both trained on the standard FAUST dataset. A visualization of the correspondence is presented in Figure 5. The results show how scaling disturbs the matching capabilities and, on some cases, have even global impact on the correspondence of Euclidean based approaches. Scale-invariant LBO excel on this dataset and even without training on locally scaled examples, managed to achieve almost the same performance as in the near-isometry case. We present quantitative analysis of the geodesic errors on 32 different pairs from the dataset in Figure 6. We must mention that we have found out that current methods are surprisingly sensitive even to minor local scale changes.

5.4. SMAL

The most significant strength of our architecture is the ability to correspond shapes from different domains, an ability we are the first to implement using unsupervised functional maps framework. We have evaluated our method on pairs of shape from the SMAL dataset [46, 45]. In Figure 1 we present a visualization for some of the inter-class results on the SMAL dataset. We can see in the results how the relaxation of the near-isometry assumption gave the model the degree of freedom to generalize itself for corresponding non-isometric shapes. On the spectral domain of the scale-invariant geometry our method managed to model inter-class relationships between shapes. We have observed how standard methods fail to converge in terms of the loss function and was giving a completely broken matches for inter-class matching.

6. Future work and Limitations

This work demonstrates the advantages in the search for alternative spectral domains for the task of shape correspondence. Without questioning the optimality of the Laplace-Beltrami operator for spanning such spectral domains, we show how the Euclidean metric is suboptimal for the purpose of non-rigid shape correspondence. The investigation of alternative metrics should be further examined, such as the affine-invariant metric presented by Raviv *et al.* in [30]. Other task-driven optimal decompositions should also be



Figure 5. Correspondence between shapes on deformed FAUST dataset, first row is the reference shapes, second row is the correspondence using scale-invariant LBO $\alpha=0.6$, third row is the correspondence using the Euclidean LBO. Scale-invariance geometry allows the architecture to be agnostic to deformations even without training on a deformed dataset.

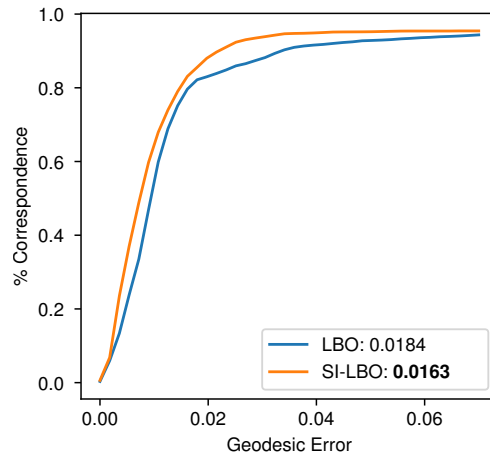


Figure 6. Error evaluation on locally scaled FAUST dataset comparing the performance of the standard and scale-invariant LBO on SURFMNet[35]

considered, such as [4]. We show great improvement in the ability to correspond shapes from different domains, but we still see limited capabilities on more severe deformations (e.g., hippo and a cat), but we believe we set another step toward a fully general non-rigid shape correspondence method.

7. Conclusions

We have realized end-to-end architecture for non-rigid and non-isometric shape correspondence, based upon scale-invariant geometry. Our architecture surpasses state-of-the-art methods on standard shape correspondence benchmarks, and it is the first to solve end-to-end inter-domain correspondence problems using the functional maps paradigm, while all other spectral methods fail.

References

- [1] Yonathan Aflalo, Haim Brezis, and Ron Kimmel. On the optimality of shape and data representation in the spectral domain. *CoRR*, abs/1409.4349, 2014. 1, 2, 4
- [2] Yonathan Aflalo, Ron Kimmel, and Dan Raviv. Scale invariant geometry for nonrigid shapes. *SIAM Journal on Imaging Sciences*, 6(3):1579–1597, 2013. 2, 4
- [3] Mathieu Aubry, Ulrich Schlickewei, and Daniel Cremers. The wave kernel signature: A quantum mechanical approach to shape analysis. In *2011 IEEE International Conference on Computer Vision Workshops (ICCV Workshops)*, pages 1626–1633, Los Alamitos, CA, USA, nov 2011. IEEE Computer Society. 1
- [4] Omri Azencot and Rongjie Lai. Shape analysis via functional map construction and bases pursuit, 2019. 8
- [5] Silvia Biasotti, Andrea Cerri, Alex Bronstein, and Michael Bronstein. Recent trends, applications, and perspectives in 3d shape similarity assessment. In *Computer Graphics Forum*, volume 35, pages 87–119. Wiley Online Library, 2016. 1
- [6] Federica Bogo, Javier Romero, Matthew Loper, and Michael Black. Faust: Dataset and evaluation for 3d mesh registration. In *Proceedings of the IEEE Computer Society Conference on Computer Vision and Pattern Recognition*, 06 2014. 6
- [7] Vincent Borrelli, Frédéric Cazals, and Jean-Marie Morvan. On the angular defect of triangulations and the pointwise approximation of curvatures. *Computer Aided Geometric Design*, 20(6):319 – 341, 2003. 4
- [8] Amit Bracha, Oshri Halim, and Ron Kimmel. Shape Correspondence by Aligning Scale-invariant LBO Eigenfunctions. In Tobias Schreck, Theoharis Theoharis, Ioannis Pratikakis, Michela Spagnuolo, and Remco C. Veltkamp, editors, *Eurographics Workshop on 3D Object Retrieval*. The Eurographics Association, 2020. 4
- [9] Alexander Bronstein, Michael Bronstein, and Ron Kimmel. *Numerical Geometry of Non-Rigid Shapes*. Springer Publishing Company, Incorporated, 1 edition, 2008. 1
- [10] Alexander M Bronstein, Michael M Bronstein, and Ron Kimmel. Generalized multidimensional scaling: a framework for isometry-invariant partial surface matching. *Proceedings of the National Academy of Sciences*, 103(5):1168–1172, 2006. 1
- [11] Michael M. Bronstein and Iasonas Kokkinos. Scale-invariant heat kernel signatures for non-rigid shape recognition. In *2010 IEEE Computer Society Conference on Computer Vision and Pattern Recognition*, pages 1704–1711, 2010. 2
- [12] Nicolas Donati, Abhishek Sharma, and Maks Ovsjanikov. Deep geometric functional maps: Robust feature learning for shape correspondence. In *Proceedings of the IEEE/CVF Conference on Computer Vision and Pattern Recognition (CVPR)*, June 2020. 1, 2
- [13] Michal Edelman, Danielle Ezuz, and Mirela Ben-Chen. Enigma: Evolutionary non-isometric geometry matching. *ACM Trans. Graph.*, 39(4), July 2020. 2
- [14] Davide Eynard, Emanuele Rodola, Klaus Glashoff, and Michael M Bronstein. Coupled functional maps. In *2016 Fourth International Conference on 3D Vision (3DV)*, pages 399–407. IEEE, 2016. 5
- [15] Dvir Ginzburg and Dan Raviv. Cyclic functional mapping: Self-supervised correspondence between non-isometric deformable shapes. *ArXiv*, abs/1912.01249, 2019. 2, 3
- [16] Oshri Halimi, Or Litany, Emanuele Rodolà, Alexander M. Bronstein, and Ron Kimmel. Self-supervised learning of dense shape correspondence. *CoRR*, abs/1812.02415, 2018. 2, 4, 6
- [17] Kaiping He, Xiangyu Zhang, Shaoqing Ren, and Jian Sun. Deep residual learning for image recognition. *CoRR*, abs/1512.03385, 2015. 4
- [18] Qixing Huang, Fan Wang, and Leonidas Guibas. Functional map networks for analyzing and exploring large shape collections. *ACM Trans. Graph.*, 33(4), July 2014. 3
- [19] Hui Chen and Bir Bhanu. 3d free-form object recognition in range images using local surface patches. In *Proceedings of the 17th International Conference on Pattern Recognition, 2004. ICPR 2004.*, volume 3, pages 136–139 Vol.3, 2004. 1
- [20] Vladimir Kim, Yaron Lipman, and Thomas Funkhouser. Blended intrinsic maps. *ACM Transactions on Graphics (Proc. SIGGRAPH)*, 30(4), July 2011. 6
- [21] Yaron Lipman and Ingrid Daubechies. Conformal wasserstein distances: Comparing surfaces in polynomial time. *Advances in Mathematics*, 227(3):1047–1077, Jun 2011. 1
- [22] Or Litany, Tal Remez, Emanuele Rodolà, Alexander M. Bronstein, and Michael M. Bronstein. Deep functional maps: Structured prediction for dense shape correspondence. *CoRR*, abs/1704.08686, 2017. 1, 2, 3, 4, 6
- [23] Evgeni Magid, Octavian Soldea, and Ehud Rivlin. A comparison of gaussian and mean curvature estimation methods on triangular meshes of range image data. *Computer Vision and Image Understanding*, 107(3):139 – 159, 2007. 4
- [24] Facundo Mémoli and Guillermo Sapiro. A theoretical and computational framework for isometry invariant recognition of point cloud data. *Foundations of Computational Mathematics*, 5(3):313–347, 2005. 1

- [25] Facundo Mémoli. On the use of gromov-hausdorff distances for shape comparison. In *Proceedings Point Based Graphics*, pages 81–90, 01 2007. [1](#)
- [26] Dorian Nogneng and Maks Ovsjanikov. Informative descriptor preservation via commutativity for shape matching. *Computer Graphics Forum*, 36:259–267, 05 2017. [3](#), [5](#)
- [27] Maks Ovsjanikov, Mirela Ben-Chen, Justin Solomon, Adrian Butscher, and Leonidas Guibas. Functional maps: a flexible representation of maps between shapes. *ACM Transactions on Graphics (TOG)*, 31(4):1–11, 2012. [1](#), [3](#), [5](#)
- [28] Maks Ovsjanikov, Etienne Corman, Michael Bronstein, Emanuele Rodolà, Mirela Ben-Chen, Leonidas Guibas, Frederic Chazal, and Alex Bronstein. Computing and processing correspondences with functional maps. In *SIGGRAPH ASIA 2016 Courses*, pages 1–60. 2016. [3](#)
- [29] Jonathan Pokrass, Alexander M Bronstein, Michael M Bronstein, Pablo Sprechmann, and Guillermo Sapiro. Sparse modeling of intrinsic correspondences. In *Computer Graphics Forum*, volume 32, pages 459–468. Wiley Online Library, 2013. [3](#)
- [30] Dan Raviv and Ron Kimmel. Affine invariant geometry for non-rigid shapes. *International Journal of Computer Vision*, 111(1):1–11, Jan 2015. [7](#)
- [31] Martin Reuter, Silvia Biasotti, Daniela Giorgi, Giuseppe Patanè, and Michela Spagnuolo. Discrete laplace–beltrami operators for shape analysis and segmentation. *Computers & Graphics*, 33(3):381 – 390, 2009. IEEE International Conference on Shape Modelling and Applications 2009. [4](#)
- [32] Emanuele Rodolà, Luca Cosmo, Michael M Bronstein, Andrea Torsello, and Daniel Cremers. Partial functional correspondence. In *Computer Graphics Forum*, volume 36, pages 222–236. Wiley Online Library, 2017. [3](#)
- [33] Emanuele Rodolà, Michael Moeller, and Daniel Cremers. Point-wise map recovery and refinement from functional correspondence. *arXiv preprint arXiv:1506.05603*, 2015. [5](#)
- [34] Steven Rosenberg. *The Laplacian on a Riemannian Manifold: An Introduction to Analysis on Manifolds*. London Mathematical Society Student Texts. Cambridge University Press, 1997. [5](#)
- [35] Jean-Michel Roufousse and Maks Ovsjanikov. Unsupervised deep learning for structured shape matching. *CoRR*, abs/1812.03794, 2018. [1](#), [2](#), [3](#), [4](#), [5](#), [6](#), [7](#)
- [36] Szymon Rusinkiewicz. Estimating curvatures and their derivatives on triangle meshes. In *2nd International Symposium on 3D Data Processing, Visualization and Transmission (3DPVT 2004), 6-9 September 2004, Thessaloniki, Greece*, pages 486–493. IEEE Computer Society, 2004. [4](#)
- [37] Raif M Rustamov, Maks Ovsjanikov, Omri Azencot, Mirela Ben-Chen, Frédéric Chazal, and Leonidas Guibas. Map-based exploration of intrinsic shape differences and variability. *ACM Transactions on Graphics (TOG)*, 32(4):1–12, 2013. [5](#)
- [38] Samuele Salti, Federico Tombari, and Luigi Di Stefano. Shot: Unique signatures of histograms for surface and texture description. *Computer Vision and Image Understanding*, 125:251 – 264, 2014. [1](#), [4](#)
- [39] R.K. Singh and J.S. Manhas. *Composition Operators on Function Spaces*. ISSN. Elsevier Science, 1993. [5](#)
- [40] Jian Sun, Maks Ovsjanikov, and Leonidas Guibas. A concise and provably informative multi-scale signature based on heat diffusion. *Computer Graphics Forum*, 28(5):1383–1392, 2009. [1](#)
- [41] Gary KL Tam, Zhi-Quan Cheng, Yu-Kun Lai, Frank C Langbein, Yonghuai Liu, David Marshall, Ralph R Martin, Xian-Fang Sun, and Paul L Rosin. Registration of 3d point clouds and meshes: A survey from rigid to nonrigid. *IEEE transactions on visualization and computer graphics*, 19(7):1199–1217, 2012. [1](#)
- [42] Oliver Van Kaick, Hao Zhang, Ghassan Hamarneh, and Daniel Cohen-Or. A survey on shape correspondence. In *Computer Graphics Forum*, volume 30, pages 1681–1707. Wiley Online Library, 2011. [1](#)
- [43] Jörg Vollmer, Robert Mencl, and Heinrich Mueller. Improved laplacian smoothing of noisy surface meshes. In *Computer graphics forum*, volume 18, pages 131–138. Wiley Online Library, 1999. [4](#)
- [44] Andrei Zaharescu, Edmond Boyer, and Radu Horaud. Key-points and local descriptors of scalar functions on 2d manifolds. *International Journal of Computer Vision*, 100(1):78–98, Oct 2012. [1](#)
- [45] Silvia Zuffi, Angjoo Kanazawa, and Michael J. Black. Lions and tigers and bears: Capturing non-rigid, 3d, articulated shape from images. In *2018 IEEE/CVF Conference on Computer Vision and Pattern Recognition*, pages 3955–3963, 2018. [7](#)
- [46] Silvia Zuffi, Angjoo Kanazawa, David W. Jacobs, and Michael J. Black. 3d menagerie: Modeling the 3d shape and pose of animals. *2017 IEEE Conference on Computer Vision and Pattern Recognition (CVPR)*, Jul 2017. [7](#)